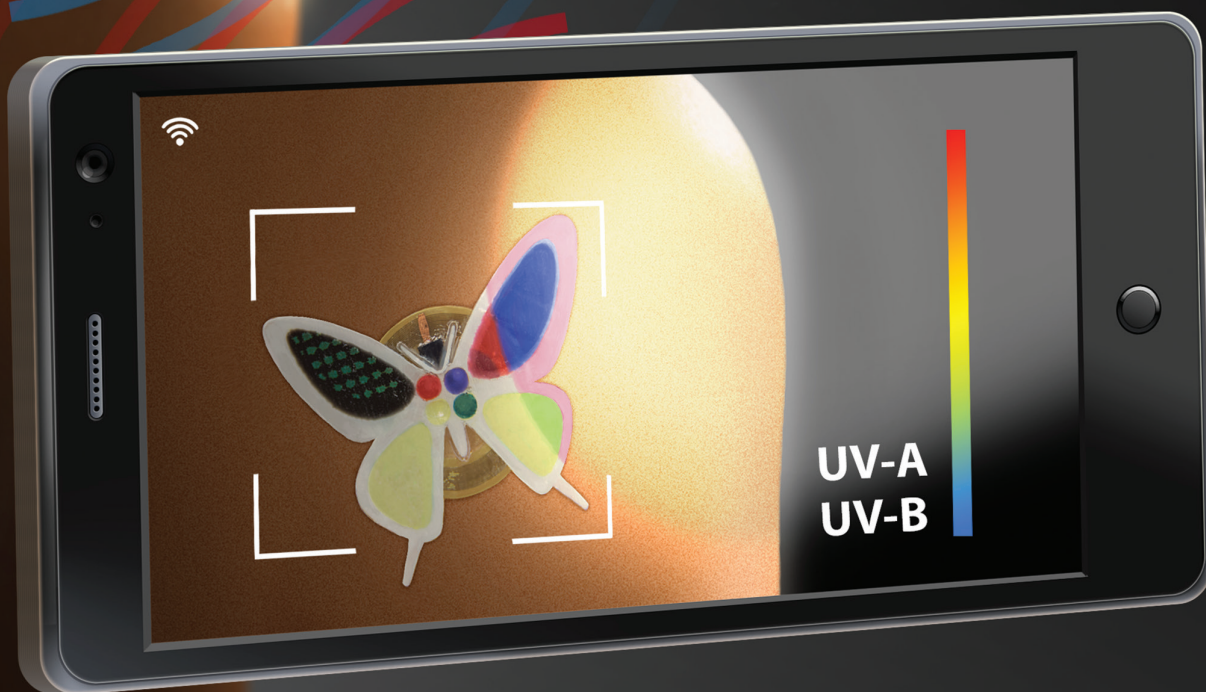


ADVANCED FUNCTIONAL MATERIALS



Materials and Device Designs for an Epidermal UV Colorimetric Dosimeter with Near Field Communication Capabilities

Hitoshi Araki, Jeonghyun Kim, Shaoning Zhang, Anthony Banks, Kaitlyn E. Crawford, Xing Sheng, Philipp Gutruf, Yunzhou Shi, Rafal M. Pielak, and John A. Rogers*

Ultraviolet (UV) solar radiation is a leading cause of skin disease. Quantitative, continuous knowledge of exposure levels can enhance awareness and lead to improved health outcomes. Devices that offer this type of measurement capability in formats that can seamlessly integrate with the skin are therefore of interest. This paper introduces materials, device designs, and data acquisition methods for a skin-like, or “epidermal,” system that combines colorimetric and electronic function for precise dosimetry in the UV-A and UV-B regions of the spectrum, and for determination of instantaneous UV exposure levels and skin temperature. The colorimetric chemistry uses (4-phenoxyphenyl)diphenylsulfonium triflate (PPDPS-TF) with crystal violet lactone (CVL) and Congo red for UV-A and UV-B operation, respectively, when integrated with suitable optical filters. Coatings of poly(ethylene-vinylacetate) (PEVA) protect the functional materials from sunscreen and other contamination. Quantitative information follows from automated $L^*a^*b^*$ color space analysis of digital images of the devices to provide accurate measurements when calibrated against standard nonwearable sensors. Techniques of screen printing and lamination allow aesthetic designs and integration with epidermal near field communication platforms, respectively. The result is a set of attractive technologies for managing UV exposure at a personal level and on targeted regions of the body.

(erythema,^[2] cataracts,^[3] melanoma,^[4] suppression of the immune system^[5])^[6] effects of UV exposure are ongoing. Above all, skin cancer, one of the most serious negative effects, represents a major health concern for people around the world. An increased level of awareness to UV exposure can be achieved by providing a convenient way for individuals to perform UV dosimetry, preferably in a direct manner, on their skin. For accurate measurements and seamless integration, the sensor platform should be rendered in a skin-compatible, wearable format, capable of long-term (i.e., days), nonirritating integration with the skin, at various positions across the body. Further, the device should be compatible with outdoor activities such as swimming, running, and bathing and with chemical components of common lotions, sunscreens, powders, and cosmetics. Commercially available digital UV sensors provide accurate data (i.e., Microsoft band2, Microsoft Corp.), but they mount on wristbands and involve mechanically hard components that are

incompatible with the direct application of sunscreen. In addition, their form factors and cost structures prevent use in many activities that are performed in the sun. Commercially available colorimetric sensors, also in wristband formats (i.e., Smartsun,

1. Introduction

Effects of UV radiation on the human body are well established. Efforts to increase public awareness of both the positive (mental wellness, vitamin D synthesis)^[1] and negative

Dr. H. Araki, Dr. J. Kim, S. Zhang, A. Banks, Dr. K. E. Crawford, Dr. P. Gutruf, Prof. J. A. Rogers
Department of Materials Science and Engineering
Frederick Seitz Materials Research Laboratory
University of Illinois at Urbana–Champaign
Urbana, IL 61801, USA
E-mail: jrogers@illinois.edu

Dr. H. Araki
Electronic and Imaging Materials Research Laboratories
Toray Industries, Inc.
Otsu, Shiga 520-0842, Japan

Prof. X. Sheng
Department of Electronic Engineering
Tsinghua University
Beijing 100084, China

Dr. P. Gutruf, Prof. J. A. Rogers
Department of Materials Science and Engineering
Northwestern University
Evanston, IL 60208, USA

Dr. Y. Shi, Dr. R. M. Pielak
L'Oréal California Research Center
San Francisco, CA 94107, USA

Prof. J. A. Rogers
Departments of Biomedical Engineering
Chemistry, Neurological Surgery
Mechanical Engineering
Electrical Engineering and Computer Science
Simpson Querrey Institute and Feinberg School of Medicine
Center for Bio-Integrated Electronics
Northwestern University
Evanston, IL 60208, USA



DOI: 10.1002/adfm.201604465

Intellego Technologies), circumvent some of these drawbacks, but their degree of accuracy is limited.

“Epidermal electronics”^[7] represents a relatively recent class of technology with the potential to offer advantages over these alternatives. Such devices are thin and soft and they are conformal to the skin. Past work demonstrates their utility in measuring various body signals such as electrocardiograms, electromyograms, strain, temperature, hydration, and many others, with additional capabilities emerging, at an accelerating rate, from ongoing research in laboratories worldwide.^[8–10] These electronics take the form of temporary transfer tattoos, with durable, long-term (up to two weeks) intimate interfaces to the skin. Additionally, these systems, like more conventional types of wearable sensors, can be mounted on clothing, wrist bands, straps, and other platforms.^[11,12] Recent reports describe methods for integrating low cost, wireless functionality based on near field communication (NFC) technology.^[13,14] The combination of simple UV sensing capabilities with this type of wireless interface, all in an epidermal format, could offer interesting possibilities, complementary to those provided by recently reported classes of flexible, hard-wired UV sensors based on the electrical responses of various deposited or printed semiconductor materials or devices.^[15–18]

Herein, we describe materials, device designs, and data acquisition approaches for colorimetric epidermal UV dosimeters that integrate NFC capabilities. Specially tailored, irreversible UV colorimetric chemistries that offer selective sensitivity in both the UV-A and UV-B regions of the spectrum and have low modulus, elastic properties in thin film geometries represent the core content. These material systems combine functional components that serve as photoactivators, color changeable dyes, and absorptive optical filters, while maintaining flexibility and stretchability for optimized conformal contact. The UV energy extraction algorithm relies on digital image capture and analysis using an external device activated by proximity to the NFC electronics. Screen printing provides a cost effective means to pattern the active components into aesthetic designs optimized for this color analysis. Compatibility with thermochromic liquid crystals and reversible UV responsive materials expands the functionality to include measurements of temperature and instantaneous UV exposure. **Figure 1** presents schematic illustrations and a digital image of the fully integrated, multifunctional device.

2. Result and Discussion

2.1. UV Dosimeter

Figure 1 presents an overview of a butterfly-shaped epidermal device that exploits four colorimetric sensors and an

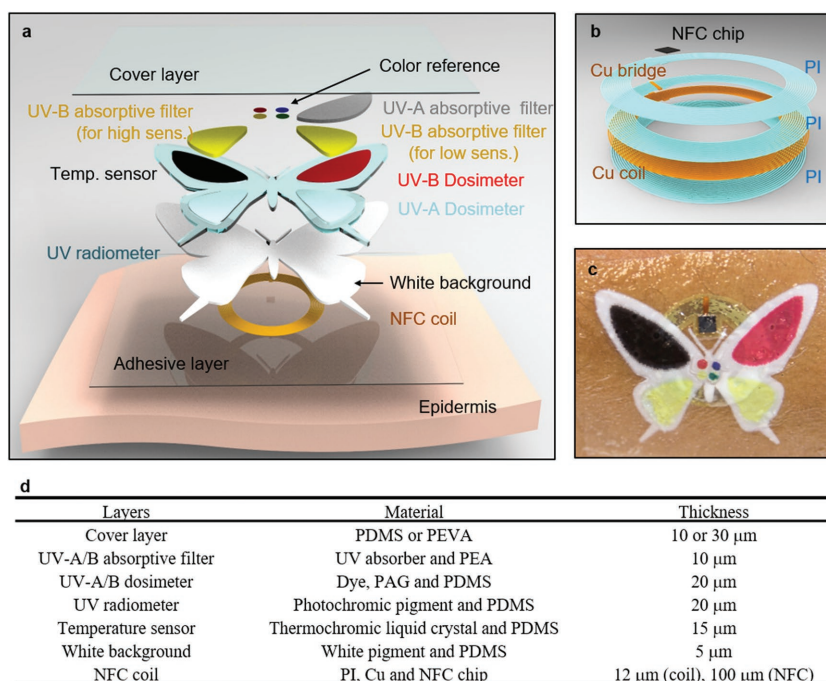


Figure 1. Schematic illustrations and digital image of a multimodal, colorimetric epidermal device with capabilities in UV and temperature sensing and in wireless operation via near field communication (NFC) electronics. a) Exploded-view schematic illustration of the various functional layers in a representative system. b) Schematic illustration of the NFC electronics, including an integrated temperature sensor. c) Image of a device on the skin. d) Table of materials and thicknesses for each layer in this system.

NFC device, described in detail in subsequent sections. The chemistry for the UV dosimeter involves irreversible, systematic changes in color that result from exposure to UV light. The material combines a photosensitive activator and a color changeable dye (**Figure 2a**). Absorption of UV photons by the photosensitive activator generates an activated species that then induces a change in the color of the dye. Representative photosensitive activators include photoacid generators (PAGs) and photoradical initiators. PAGs are in widespread use in chemically amplified photoresists designed for semiconductor manufacturing.^[19] Photoradical initiators are found in many UV curable materials.^[20] The color changeable dyes include leuco dyes as pH indicators for PAGs and dyes that decompose when exposed to radical species for photoradical initiators. Here, the leuco dyes change from colorless to brightly colored forms with decreasing pH. When embedded in a soft elastomeric matrix material, such as polydimethyl siloxane (PDMS), this colorimetric system offers low modulus and skin conformal mechanics, with adjustable, high sensitivity to UV exposure. Moreover, the versatility of the chemistry allows access to a wide range of colors, by use of different dyes and/or inactive color additives. UV-A and -B sensing can be achieved by integration of an optical filter layer to control the sensing wavelength (**Figure 3a–d**). The overall dynamic range for sensing associated with various skin types can be controlled with a separate optical filter (**Figure 3e**, Section 2.3).

The UV colorimetric material described here for UV-A dosimetry uses crystal violet lactone (CVL) as the leuco dye,

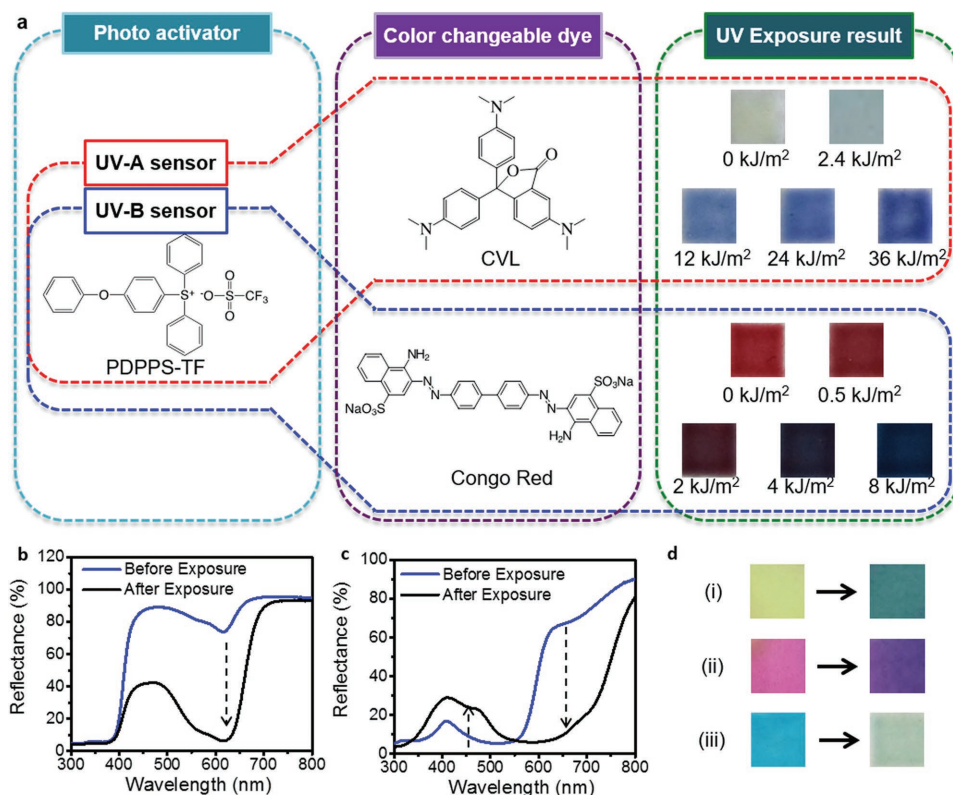


Figure 2. Chemistry and response of stretchable materials for colorimetric UV dosimetry. a) Chemical structure and the result of UV exposure. PPDPS-TF and CVL provide for sensing in the UV-A band. PPDPS-TF and Congo red provide for sensing in the UV-B band. b) UV–vis reflection spectra of PPDPS-TF and CVL mixed into a PDMS matrix, before and after exposure (thickness = 30 μm , exposure time = 10 min (by UV-A lamp, intensity = 22 W m^{-2})). c) UV–vis reflection spectra of PPDPS-TF and Congo red mixed into a PDMS matrix before and after exposure (thickness = 30 μm , exposure time = 10 min (by UV-B lamp, intensity = 5 W m^{-2})). d) Color diversity enabled by these chemistries. The left side is before exposure and the right side is after exposure. (i) Yellow to green transition associated with a material that consists of PPDPS-TF, CVL, and yellow pigment, with exposure condition identical to that in (b). (ii) Magenta to violet transition associated with a material that consists of PPDPS-TF and CVL and magenta pigment, with exposure condition identical to that in (b). (iii) Blue to colorless transition associated with a material that consists of Direct Blue 86 and Irgacure 2959, with exposure condition identical to that in (c).

and (4-phenoxyphenyl)diphenylsulfonium triflate (PPDPS-TF) as the PAG. Exposure of CVL to acidic conditions opens the lactone ring and initiates a color change to blue. A stretchable, screen-printable formulation includes PDMS as a binder polymer for the CVL and PPDPS-TF. Films with thicknesses in the range of $\approx 20 \mu\text{m}$ can be screen printed onto substrates such as films of polyethylene terephthalate (PET). Figure 2b shows the UV–vis reflection spectra of the CVL-PPDPS-TF material before and after exposure to UV-A (lamp UVL-26, UVP LLC). The reflection feature at $\approx 600 \text{ nm}$ decreases by an amount that is directly proportional to the exposure dose (Figure 2a, right). Although UV absorption by PPDPS-TF occurs at wavelengths shorter than 320 nm (Figure S1a, Supporting Information), the overall CVL-PPDPS-TF material has a sensitivity that extends to substantially longer wavelengths. This behavior follows from the role of CVL as a sensitizer for the response of PPDPS-TF. Experiments to illuminate these effects involve exposure with broadband UV light (solar simulator, Newport) passed through UV long pass filters that eliminate wavelengths below 380 nm (Filter-1) and 430 nm (Filter-2) (Figure S1a, Supporting Information). The color response of CVL is unaffected

by the presence of Filter-1, but is eliminated with Filter-2 (Figure S1b, Supporting Information). This result is consistent with a wavelength sensitivity between 380 and 430 nm. A filter that absorbs UV-B and violet light, but is transparent in the range between 315 and 400 nm offers sensitivity to UV-A wavelengths (Figure 3a). Figure 3b,d shows UV–vis spectra of the UV-B and violet light absorptive filter, where the material composition is a mixture of a UV absorber (ABS-409, Exciton) and ethylhexyl triazone (Uvinul T150, BASF) and poly(ethylacrylate) (PEA) (see section “UV-B and Violet Light Absorptive Filter” in the Experimental Section), and the response of the UV-A sensing material exposure to UV-A and UV-B, respectively. Figure 2d (i) and (ii) demonstrates a color tuning result with paint that has yellow (Silc Pig Yellow, Smooth-On) and magenta (Oil Color Paint Quinacridone Magenta, Winsor & Newton Artists) pigment, respectively, when mixed at 2 wt% with PDMS.

The material for UV-B dosimetry includes Congo red (dye as pH indicator, changing from red at $\text{pH} > 5.2$ to blue at $\text{pH} < 3.0$), PPDPS-TF (PAG), and PDMS (binder polymer). Figure 2c shows UV–vis reflection spectra collected before and after exposure to UV-B (lamp UVM-26, UVP LLC). The reflection feature

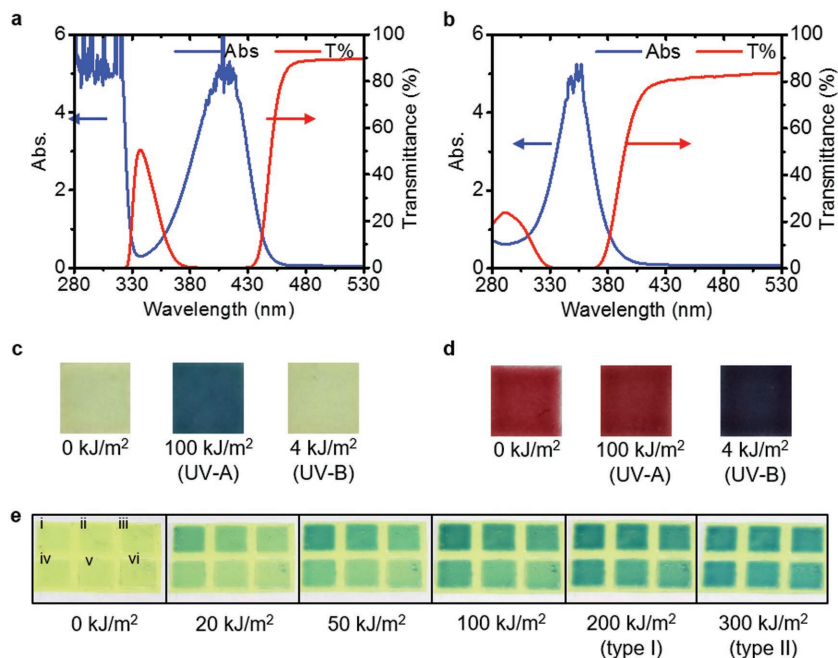


Figure 3. Experimental results for the behaviors of UV-A and UV-B stretchable colorimetric dosimeter materials and sensitivity control. UV-vis absorption spectra of a) UV-B and violet light absorptive filters and b) UV-A absorptive filter. Digital images of c) UV-A dosimeter and d) UV-B dosimeter before and after exposure using UV-A and UV-B lamps. e) 3×2 array of UV-A dosimeter materials with or without a UV-A absorptive filter to control the sensitivity: (i) no filter, (ii)–(vi) 1–5 UV-A absorptive filters (Figure S9, Supporting Information).

at ≈ 650 nm decreases and at ≈ 450 nm increases. Since Congo red does not work as a sensitizer of PPDPS-TF, this material responds to wavelengths defined by the PPDPS-TF alone, i.e., mainly to UV-B since the absorption edge of PPDPS-TF is 324 nm, sensitivity of the chemical overlaps between UV-A and UV-B. Addition of a thin film that absorbs UV-A can further enhance a selective response to UV-B. Figure 3c shows the UV-vis spectrum of this filter with a material composition set as a mixture of a UV absorber (diethylamino hydroxybenzoyl hexyl benzoate, Uvinul A plus Granular, BASF) and PEA (see section “UV-A Absorptive Filter” in the Experimental Section). Figure 3e shows the UV-vis spectrum of the response of the UV-B dosimeter material. A mixture of Direct blue 86 (dye), Irgacure 2959 (photoradial initiator), avobenzene (UV-A absorber), PDMS (binder polymer), and diethyleneglycol (DEG) (solvent) offers an alternative formulation for UV-B dosimetry. This system provides color transitions opposite to those provided by the leuco dye and PAG formulation (Figure 2d (iii) and Figure S7 (Supporting Information)).

2.2. Sensitivity Control

The minimal erythral dose (MED) corresponds to the minimum UV dose that produces reddening of the skin within 1–6 h but which disappears in 24 h. The MED depends on skin type, as summarized in Table S1 (Supporting Information).^[2] The range of sensitivity of a UV dosimeter should match the MED values for the targeted skin type. The addition of UV

filter layers can provide the necessary control. Measurements on a screen-printed 3×2 array of square patterns of UV-A sensing material uniformly covered with a UV-B filter and with a different number (0–5) of stacked UV-A filters in each area from (i) to (iv) in Figure 3e illustrate this type of control (Absorption spectra of the stacked filters appear in Figure S9 in the Supporting Information). Results from this array demonstrate the ability to tailor the response across relevant ranges for all skin types.

2.3. Image Analysis

Images of the devices captured with a digital camera can be quantitatively analyzed to determine the change in color and, with appropriate calibration, the exposure dose. Analysis relies on $L^*a^*b^*$ (CIE 1976 source = D65) color space parameters, where L^* represents the lightness and a^* and b^* the color-opponent dimensions. Any given color represents a single point in this 3D parameter space. The degree of difference between two colors, ΔEab , corresponds to the distance between two points in the $L^*a^*b^*$ color space. The value of ΔEab can be calculated according to ref. [21]

$$\Delta Eab_x = \left[(L_0^* - L_x^*)^2 + (a_0^* - a_x^*)^2 + (b_0^* - b_x^*)^2 \right]^{1/2} \quad (1)$$

where L_0^* , a_0^* , b_0^* and L_x^* , a_x^* , b_x^* are values for unexposed (dose of 0 kJ m^{-2}) and exposed (dose of $x \text{ kJ m}^{-2}$) material, respectively. The value of ΔEab increases monotonically with dose, in a manner that can be calibrated to yield quantitative information. The 3D matrices of an image can be calculated from standard Red, Green, and Blue color space (sRGB) parameters extracted using standard image analysis software (Photoshop CC2015, Adobe). In the procedures used here, a given area of interest yields a single averaged value of sRGB, to minimize the effects of spatial nonuniformities in the color (Figure S2c,f, Supporting Information). Conversion to $L^*a^*b^*$ color space proceeds from these sRGB data. A demonstration involves pictures of a 3×3 printed array of square patterns of UV colorimetric material collected under illumination with white fluorescence lighting and incandescent light sources, after exposure to various doses of UV (Figure 4a and Figure S2a,b,d,e (Supporting Information)). The calibration process involves two steps: (1) Normalizing each ΔEab by the value of the saturated developed color (Table S2, Supporting Information), to eliminate effects of illumination condition. (2) Comparing the normalized value of the inverse of ΔEab to the inverse of the exposure dose ($=x$) and this relationship to the expected behavior according to a standard saturation model (Equation (2)). Figure 4b reveals a linear relationship between $1/\Delta Eab$ and $1/x$ for different illumination conditions, with nearly identical functional forms

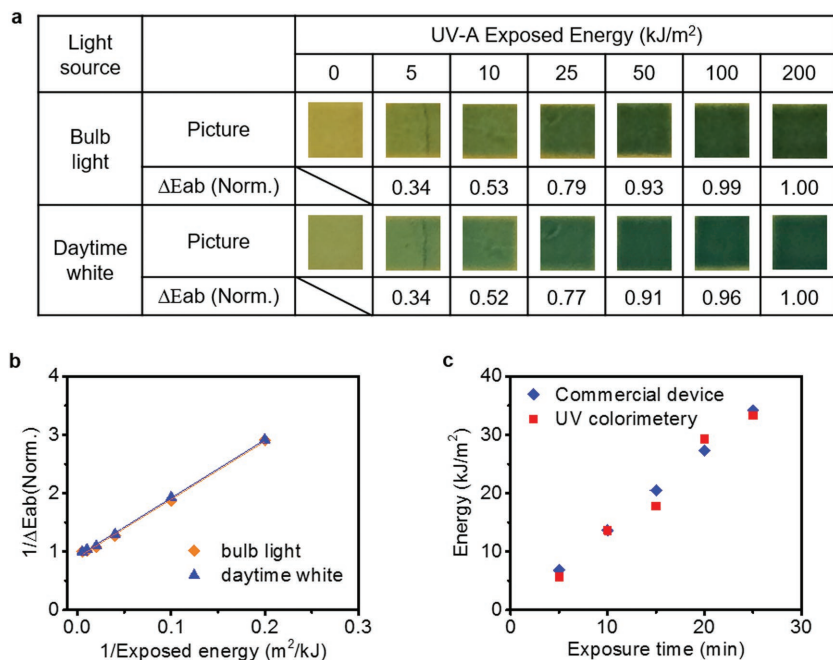


Figure 4. Methods for image analysis to determine the exposure dose from changes in color. a) Image and normalized value of ΔEab for the UV-A colorimetric dosimeter material after exposure with various energies ($\Delta Eab_x(\text{Norm.}) = \Delta Eab_x/\Delta Eab_{200}$). The images here were collected under incandescent light and daylight white fluorescent light. b) Plot of $1/x$ ($x =$ exposed energy) versus $1/\Delta Eab_x$ (Norm.). c) Results for UV measurement of sunlight in Urbana, IL, USA (at 2/27/2016 11:40–12:00 weather condition was sunny) using a commercial device and the UV colorimetric material. Calibration of the material was performed using a solar simulator (Newport).

$$1/x = A 1/\Delta Eab_x + B \quad (2)$$

where A and B are constants determined from calibration experiments.

Functional demonstrations involve comparisons between quantitative data extracted in this manner using the UV-A sensing material (calibrated using light from a solar simulator, Table S5 and Figure S5 (Supporting Information)) and those collected with a commercial UV digital sensor (Solarmeter models 5 and 6, Solartech Inc.), under sunlight illumination during sunny conditions (2/27/2016 11:40–12:05 at Urbana IL, USA). UV-A exposure doses are inferred from data measured by Solarmeter model 5 (UV-A+B) and Solarmeter model 6 (UV-B). Image capture and digital sensor readings occurred in 5 and 1 min intervals, respectively. The measurement results exhibit quantitative agreement (Figure 4c and Tables S4 and S6 (Supporting Information)).

2.4. UV Radiometer

Capabilities in colorimetric UV radiometry can be included by use of commercially available microencapsulated photochromic pigments (photochromic powder red #19,

Hallcrest) dispersed in a PDMS binder by planetary and centrifugal mixing (ARE-310, THINKY). Here, the pigment changes from colorless to red upon absorption of UV-A and -B (mainly UV-A) by an amount that depends on the intensity. **Figure 5a** shows the color immediately after UV-A exposure (lamp UVL-26, UVP LLC) for 20 s at intensities of 45, 36, 29, 23, 18, 9, 6, and 0.6 W m^{-2} . Increasing the UV intensity increases the magenta coloration. Return to a colorless state occurs spontaneously after removal of UV light.

2.5. Temperature Sensor

Capabilities in colorimetric temperature sensing can be included by exploiting microencapsulated liquid crystal materials and techniques reported previously.^[22] The helical pitch of the liquid crystal determines the wavelength of reflected light, and this pitch is sensitive to temperature.^[23,24] **Figure 5b** shows an image of a screen printed array of square regions (900 μm separated by 400 μm) of this material (SSN200R33C5W, Hallcrest. Color change range is 33–38 °C). Contact with a finger from the backside of the substrate induces changes in color from red to green and blue. The untouched area remains black. A separate temperature sensing capability follows from the digital sensor embedded in the NFC chip. Such measurements can provide an alternative to the colorimetric readout approach, with particular value for cases where the temperature falls outside of the range of maximum response of the liquid crystal material. Since the response of UV sensing materials depends slightly on temperature across a physiologically relevant range, integration of this type of temperature sensing can facilitate precise calculation of UV dose (Figure S8, Supporting Information).

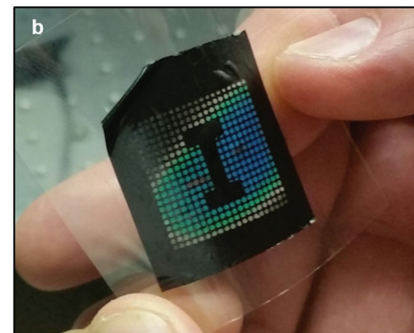
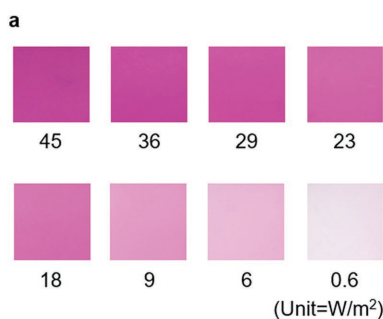


Figure 5. Images of the color response of stretchable materials for UV radiometry and the operation of a liquid crystal based colorimetric temperature sensor. a) Digital images of the UV colorimetric radiometer material captured just after UV-A exposure at intensities of 45, 36, 29, 23, 18, 9, 6, 0.6 W m^{-2} . b) Image of a patterned pixel array of thermochromic liquid crystal formed by screen printing on a film of PET.

2.6. Integrated System, with Epidermal Electronics

As highlighted previously, Figure 1a presents an exploded view schematic illustration of a butterfly shaped epidermal device that exploits all of these materials in four colorimetric sensors: (1) UV-A dosimeter made from leuco dye and PAGs in PDMS. The left and right bottom areas are for high and low sensitivity measurement, respectively, achieved by use of different optical filters (Figure S13, Supporting Information). Additional filter layers can alter the change in color from colorless to blue, to yellow to green, (2) UV-B dosimeter made from Congo red and PAGs in PDMS (upper right area, red to blue), (3) UV radiometer made from photochromic compounds in PDMS (frame area, white to red), (4) temperature sensor made from thermochromic liquid crystal in black PDMS (upper left area, black to red, green, and blue). Here, because the performance of the UV-A dosimeter layer can be affected by direct contact with the UV absorber (ABS-409, Exciton), we use a separating film ($\approx 25 \mu\text{m}$) of a transparent polymer (polyisobutylene, PIB; BASF). Color references for image analysis include small regions with dye, but without PAG, and with fumed silica (5% in PDMS). A thin ($\approx 25 \mu\text{m}$) medical adhesive (acrylic adhesive, Scapa Healthcare) bonds the system to the skin.

An epidermal NFC device shown in Figure 1b provides a wireless interface to an external reader such as a smartphone and can be easily integrated in the system because of its thin geometry, low mass, and small overall size ($<20 \mu\text{m}$, $<10 \text{ mg}$, and 16 mm diameter).^[13] The resulting platform can offer a wide range of functions, but here it specifically automates the process of launching the image capture and analysis software and records a digital reading of temperature.^[14,25] An image of a full, integrated system on the skin appears in Figure 1c. The images of Figure 6b and the Movies S1 and S2 (Supporting Information) demonstrate this functionality.

Figure 6c illustrates the ability of this system to conform to the surface of the skin, in a way that is compatible with natural deformations of the skin, a critically important feature of the device. Figure 6d shows strain–stress behaviors of key constituent materials measured by dynamic mechanical analysis (DMA-Q800, TA instrument) in tensile mode. The Young's modulus of PDMS(10:1), PDMS(30:1), adhesive, PIB, and UV sensing material are 2.2, 0.28, 0.02, 0.51, and

0.55 MPa, respectively. The combination of these materials into a single platform yields a system with soft, skin-compatible mechanics.

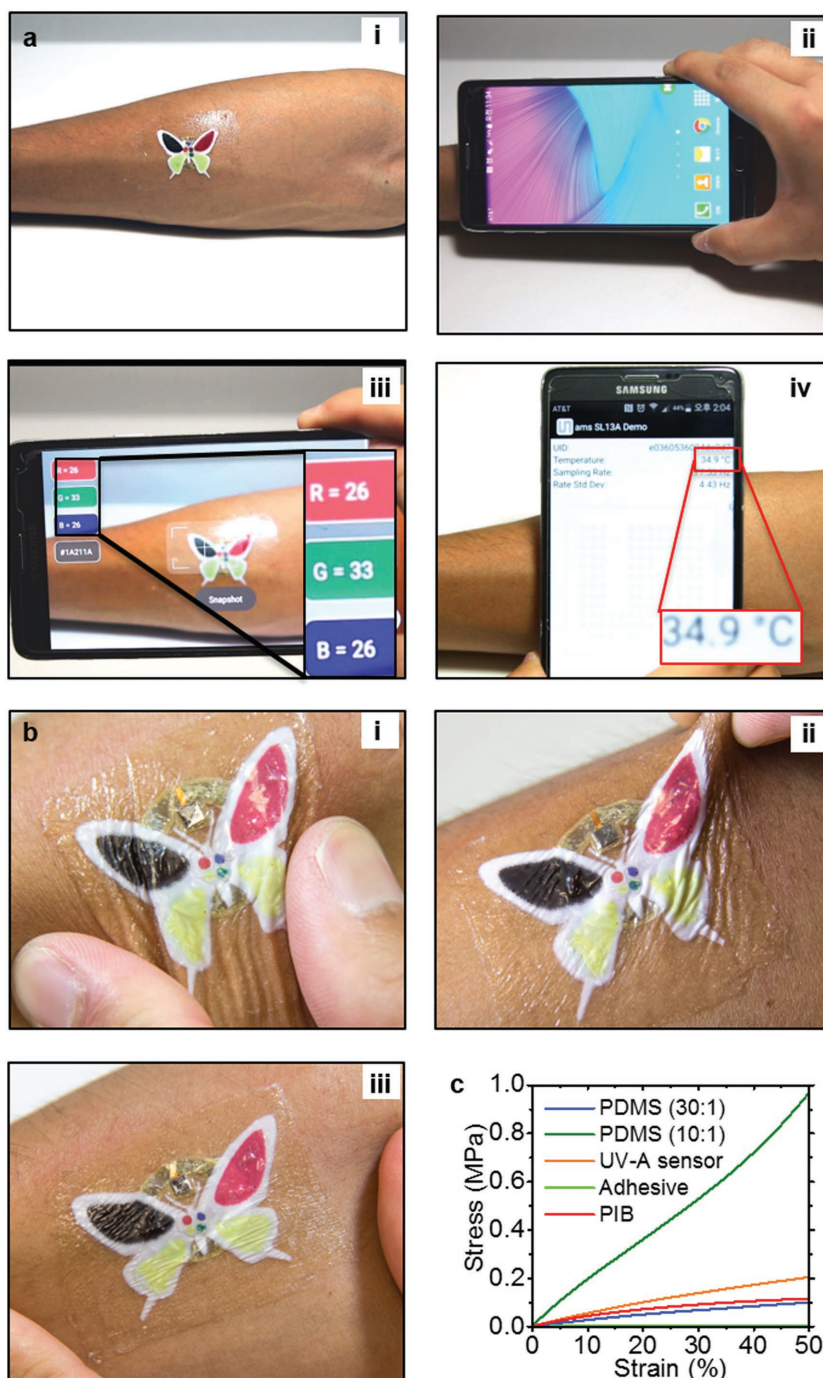


Figure 6. Images of device functionality, skin conformability, and stretchable mechanical properties of the constituent materials. a) Series of images demonstrating wireless communication with a smartphone for image capture and analysis: (i) device on the forearm, (ii) wireless communication with the device, (iii) image analysis for extraction of RGB parameters (captured from Movie S1, Supporting Information). (iv) temperature readout with smartphone (captured from Movie S2, Supporting Information). b) Series of image demonstrating skin conformability: (i) compressed, (ii) pinched, and (iii) stretched. c) Stress–strain curves for materials used in each layer.

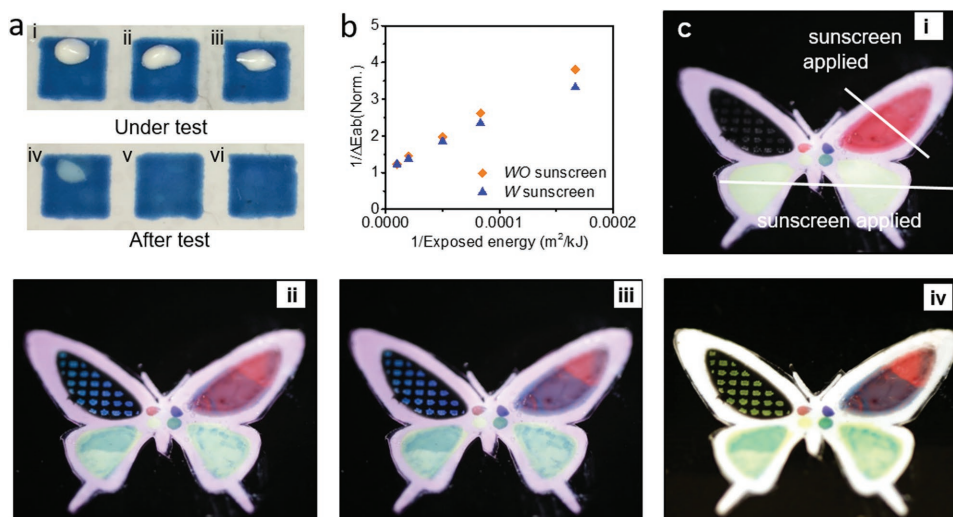


Figure 7. Image of the device functionality and its skin conformability. a) Pictures after sunscreen durability tests with protection layers: ((i and iv) PDMS, (ii and v) PE, (iii and vi) PEVA). b) Results of image analysis with and without sunscreen. c) Images of a butterfly shaped device under exposure: (i) early, (ii) midterm, and (iii) later stage. (iv) Image of a butterfly patch after exposure with a solar simulator (UV-A intensity = 11 W m⁻², UV-B intensity = 1.0 W m⁻², exposure time = 40 min).

2.7. Protection Layers for Sunscreen Durability

Certain applications benefit from encapsulation layers to ensure compatibility with sunscreens, lotions, and other materials that might come into contact with the skin, and to physically protect the devices against mechanical abrasion. Candidates include elastomers such as PDMS and thermoplastic polyurethane (TPU), but the latter absorbs UV-B (Figure S6, Supporting Information) and the former is not sufficiently impermeable. Polyethylene (PE) and poly(ethylene-vinylacetate) (PEVA) films (vinylacetate (VA) ratio = 5%, thickness = 30 μm, Young's modulus = 118 MPa) (Figure S10, Supporting Information) do not have either of these deficiencies (Figure 7a and Figure S11 (Supporting Information)). PEVA is preferred due to its elastic properties. Demonstrations of compatibility with sunscreen cream involved application directly onto PEVA-coated UV-A sensing material. Removal of the sunscreen after 8 h followed by tests of sensitivity to UV exposure indicate little or no change in response (Figure 7b and Figure S4 (Supporting Information)). Sunscreen cream applied and spread on a UV-A colorimetric dosimeter protected by PEVA allows evaluation of the efficacy of sunscreens. In a simple example, application of sunscreen decreased the transmitted UV-A energy by a factor of three (Figure S16, Supporting Information). Images in Figure 7c and Movie S3 (Supporting Information) show color transitions due to UV exposure of a device with a PEVA protection layer. The white lines in the bottom and upper right regions of Figure 7c-i correspond to areas with applied sunscreen. The white frame in this butterfly design changes to magenta under exposure. Colors of the three dosimeter regions change in a gradual manner, quantitatively determined by exposure dose, as expected; the regions coated with sunscreen undergo negligible change, also as expected.

3. Conclusion

Stretchable materials for UV colorimetric sensing (dosimeters and radiometers) and temperature sensing, taken together with NFC electronics and associated digital image analysis procedures serve as the basis for epidermal devices that can aid in the measurement, and therefore management, of exposure to UV. The UV sensing materials combine photoactivators (PPDP-TF) and color changeable dye (CVL and Congo red) in an elastomeric matrix of PDMS, where the addition of stretchable optical thin film filters can control overall sensitivity and spectral responsivity to UV-A and UV-B. Overall breathability of the devices could, potentially, be important in the context of practical applications that involve significant perspiration. Here, the use of soft, stretchable fabricate substrates as platforms for the functional materials and devices could be useful.^[26,27] Development of similar approaches in stretchable material design may allow for sensing of additional types of environmental exposure, such as pollution, high energy radiation, chemical/biological agents, and others.

4. Experimental Section

UV Sensing Material (UV-A): A solution of CVL (20 wt%) and PPDP-TF (20 wt%) in cyclopentanone were mixed with a PDMS precursor (Sylgard 184; part A:part B = 10:1, Dow Corning) at a ratio of CVL:PPDP-TF:PDMS = 2:2.5:95.5. Platinum(0)-1,3-divinyl-1,1,3,3-tetramethyldisiloxane complex solution (20 ppm based on Pt) was mixed with Sylgard part A beforehand to enhance curing. Mixing occurred in a vortex mixer until the solution became uniform in appearance. The ink was screen printed (mesh = 110) and cured at 110 °C for 5 min on a hot plate.

UV Sensing Material (UV-B): A typical synthesis of UV-B sensing material can be described as follows: 0.016 g Congo red and 0.097 g PPDP-TF were dissolved in 7.95 g methanol (solution A). One third of

solution A was mixed in 5.16 g PDMS part A using a stirring bar. Placing the mixture in a vacuum chamber enabled removal of the methanol. This process of mixing and removing the methanol was repeated twice. The resulting solid concentration of the mixture of Congo red, PPDPS-TF, and PDMS part A was 78%. 0.52 g PDMS part B was added to the mixture, followed by mixing with a stirring bar. The mixing ratio was Congo red:PPDPS-TF:PDMS = 0.3:1.7:98. The ink was screen printed (mesh = 110) and cured at 110 °C for 5 min on a hot plate.

Pigment Dispersion in PDMS: 5 g TiO₂ white pigment (Sigma-Aldrich) and 10 g PDMS part A were placed in a plastic bottle and mixed by a planetary and centrifugal mixer (ARE-310, THINKY). Large aggregated pigments were removed by filtration (filter mesh = 635). Mixing the resulting white paste with PDMS parts A and B at a ratio of 50:50:3 yielded the precursor for white, a PDMS background to eliminate the dependence of colorimetric response and image analysis to underlying skin color. A dispersion of photochromic pigments (photochromic powder red #19, Hallcrest) in PDMS was created in a similar manner. These inks were patterned by screen printing. For tests of response to UV exposure (Figure 5a), the photochromic ink was spin cast (2000 rpm for 30 s) and cured on a hot plate at 110 °C for 5 min to yield films with thicknesses of 30 μm.

UV-B and Violet Light Absorptive Filter: Fabrication began with pressing a slab of PDMS against 30 μm-thick film of PEVA (Tamapoly Co. Ltd. "SB-5") on a glass slide heated on a hot plate at 110 °C for 2 min. This process adhered the PEVA to the glass to prevent dimensional change during thermal processing associated with subsequent steps. Poly(ethylacrylate) (PEA) (Scientific Polymer Products), ABS-409 (Exciton), and ethylhexyl triazone (Uvinul T150, BASF) were dissolved in chloroform. The mixing ratio was PEA:ABS-409:T150 = 90.5:2:7.5. The nonvolatile concentration was 40 wt%. This solution was coated on the PEVA/glass substrate and baked on a hot plate at 90 °C for 3 min. The filter layer was covered by PEVA to place it between two layers of PEVA. The PEVA film was peeled from the glass, and placed on top of the 3 × 3 array UV colorimetric material. The thickness of the coating layer was 14 μm, and the total thickness was 74 μm.

UV-A Absorptive Filter: The UV-A absorptive filter used PEA and diethylamino hydroxybenzoyl hexyl benzoate (Uvinul A plus Granular, BASF) processed in a manner similar to that for the UV-B and violet light absorptive filter.

UV-A and Violet Light Absorptive Filter: The UV-A and violet light absorptive filter used PEA and Uvinul A plus Granular (BASF) processed in a manner similar to that for the UV-B and violet light absorptive filter. The UV-A and violet light absorptive filter for UV-B exposure test used PEA, ABS-409 (Exciton), and Uvinul A plus Granular (BASF) processed in a manner similar to that for the UV-B and blue absorptive filter.

UV Exposure Test: UV-A and UV-B exposure were performed with UVL-26 and UVM-26 light sources (VVP LLC), respectively. The UV-A intensity was 14 W m⁻² for the dosimeter tests and 45 W m⁻² for the radiometer tests. The small amount of UV-A and visible light emitted by UVM-26 were removed by UV-A and violet light absorptive filters. Broadband exposure used a solar simulator (Newport) with UV-A and -B intensities of 18 and 1.7 W m⁻², respectively.

UV-Vis Measurements: UV-vis reflection spectra of UV sensing materials were collected using a spectrophotometer on white background with an integrating sphere (Cary 5000, Agilent, USA). Samples for measurement were prepared by spin casting and curing on a hot plate (110 °C for 2 min). The thicknesses were 30 μm. UV-vis absorption spectra of the UV absorptive filters were measured with a spectrophotometer without an integrating sphere (Cary G5, Agilent). Samples for measurement were prepared using procedures similar to those for the UV sensing materials (thickness = 7.5 μm).

Image Analysis: Patterned 3 × 3 arrays of a UV-A sensing material (CVL/PPDPS-TF) with UV-B and violet light absorptive filters were used for image analysis. Each array was exposed to UV-A with various doses, and images were collected with a digital camera (iPhone 5s, Apple Inc.) mounted under incandescent white light and daylight white fluorescent light (Figure S2a,b,d,e, Supporting Information). Image analysis used Photoshop CC2015 (Adobe) to extract a single averaged

value of sRGB, to minimize the effects of slight spatial nonuniformities in the color. Conversion from sRGB to L*a*b* (CIE, light source = D65) was accomplished using XYZ color parameters corresponding to CIE standards. The sRGB parameter was first converted to the linear RGB parameter, followed by conversion to the XYZ parameter.^[21] The overall conversion process from sRGB to L*a*b* is as follows.

L*a*b* parameter is defined by the following equation:

$$\begin{aligned} L^* &= 116f(Y/Y_n) - 16 \\ a^* &= 500[f(X/X_n) - f(Y/Y_n)] \\ b^* &= 200[f(Y/Y_n) - f(Z/Z_n)] \end{aligned} \quad (3)$$

Where

$$f(t) = \begin{cases} t^{1/3} & \text{if } t > \left(\frac{6}{29}\right)^3 \\ \frac{1}{3}\left(\frac{29}{6}\right)^2 t + \frac{4}{29} & \text{otherwise} \end{cases}$$

X_n = 95.047, Y_n = 100.000, Z_n = 108.883 (Illuminant = D65)

X, Y, Z parameters are defined with the following equation

$$\begin{pmatrix} X \\ Y \\ Z \end{pmatrix} = \begin{pmatrix} 0.412453 & 0.35758 & 0.180423 \\ 0.212671 & 0.71516 & 0.072169 \\ 0.019334 & 0.119193 & 0.950227 \end{pmatrix} \begin{pmatrix} R' \\ G' \\ B' \end{pmatrix} \quad (4)$$

When illuminant is D65

R', G', and B' stand for linear RGB parameters for sRGB color space. sRGB values extracted from Photoshop are nonlinear RGB parameters (gamma correction = 2.2). The relationship between nonlinear and linear RGB parameters for sRGB color space for gamma correction = 2.2 is defined by the following equation

$$R' = \begin{cases} \frac{R}{12.92} & (R \leq 0.040450) \\ \left[\frac{R + 0.055}{1.055} \right]^{2.4} \cdot 1.055 & (R \geq 0.040450) \end{cases} \quad (5)$$

R is extracted data from Photoshop

G' and B' are obtained from G and B in a similar manner.

According to Equations (3)–(5), L*, a*, b* parameters can be extracted from RGB parameters.

Comparison Test of UV Measurement: The UV-A sensing material was calibrated with a solar simulator by the image analysis method described above, where Equation (4) represented the calibration expression (Table S5 and Figure S5, Supporting Information). A sample of the colorimetric material printed on a PET film was placed on a white support, oriented horizontally, facing in the vertical direction (2/27/2016 11:40–12:05 in Urbana IL, USA). Images of the sample were collected every 5 min under shade. Unexposed and fully developed regions served as color references. A commercial digital device (Solartech models 5 and 6, Solartech Inc.) recorded the UV intensity of the incident sunlight every 1 min. Model 5 was sensitive to UV-A and -B and model 6 was sensitive to UV-B. UV-A intensity was calculated from the difference between data collected using these systems. The UV-A intensity measured by the commercial device was calculated from the maximum value collected by facing the unit toward the sun and solar altitude. The solar altitude was calculated from the length of a shadow of a pencil that stood vertically on a flat stage (Table S4a (Supporting Information) and Equation (7)). The total exposure dose was determined from accumulated intensity readings (Table S4b, Supporting Information). The results from color analysis of the UV colorimetric dosimeter and those from readings from the commercial device are in Tables S4 and

S6 (Supporting Information), respectively (red numbers in both tables appear in Figure 4c)

$$1/x = 6.2615 \times 1 / \Delta Eab_x(\text{norm.}) + 1 \quad (6)$$

x : UV-A exposed energy (kJ m^{-2})
 $\Delta Eab_x(\text{norm.})$: Normalized ΔEab at x kJ m^{-2} exposed

$$I_{\text{ver}} = I_{\text{max}} \times \cos(\pi / 2 - \theta) \quad (7)$$

I_{ver} : Intensity of vertical direction
 I_{max} : Maximum intensity
 θ : Solar altitude (radian)

Sunscreen Test-1: Tests used UV colorimetric material made from PPDPS-TF and CVL and exposure to UV-A (50 kJ m^{-2}). The material was covered by films of PDMS ($30 \mu\text{m}$), PE ($20 \mu\text{m}$), and PEVA ($30 \mu\text{m}$). Sunscreen cream (Equate Ultra protection, SPF-50) was applied to 2 mm diameter regions in the center of each film. Removing the sunscreen with a cloth after 20 h allowed comparison of the appearance of the UV colorimetric material in regions with and without applied sunscreen (Figure 7a).

Sunscreen Test-2: Manual application of sunscreen cream (Equate Ultra protection, SPF-50) on UV-A sensing material covered by PEVA and followed by removal after 8 h allowed assessment of durability to sunscreen (Figure 7b and Figure S4 (Supporting Information)).

Strain-Stress Measurement: Samples of PDMS(10:1), PDMS (30:1), UV-A sensing material, and adhesive film were prepared for measurement in tensile mode by dynamic mechanical analysis (DMA-Q800, TA instrument). Typical sample geometries were $10 \text{ mm} \times 3 \text{ mm} \times 0.03 \text{ mm}$ with a strain rate of $10\% \text{ min}^{-1}$ up to 50%.

NFC Device Fabrication: The process^[13] began with lamination of a bilayer of Cu ($5 \mu\text{m}$, Oak Mitsui Microthin series) and polyimide (PI, $2.4 \mu\text{m}$) onto a PDMS-coated glass slide. Photolithography and wet etching defined the wireless coil in the Cu, and another layer of PI ($2.4 \mu\text{m}$) provided encapsulation. Contact openings for an interconnecting bridge were defined by oxygen plasma etching. A layer of Cu ($1 \mu\text{m}$) served as an interconnecting bridge. Oxygen plasma removed unnecessary PI, leaving the PI only in the regions of the wireless coil. An In/Ag solder paste (Ind. 290, Indium Corporation) bonded an NFC chip (SL13A, ams AG) to the coil.

Supporting Information

Supporting Information is available from the Wiley Online Library or from the author.

Acknowledgements

H.A. and J.K. contributed equally to this work. This research was supported in part by funding from L'Oréal. H. Araki acknowledges financial support from Toray Industries, Inc. X. Sheng acknowledges support from the National Natural Science Foundation of China (Project 51602172).

Received: August 29, 2016

Revised: September 26, 2016

Published online: November 15, 2016

[1] M. B. Humble, *J. Photochem. Photobiol.*, **B 2010**, 101, 142.

[2] T. B. Fitzpatrick, *Arch. Dermatol.* **1988**, 124, 869.

[3] H. R. Taylor, S. K. West, F. S. Rosenthal, B. Munoz, H. S. Newland, H. Abbey, E. A. Emmett, *N. Engl. J. Med.* **1988**, 319, 1429.

[4] F. Urbach, *J. Photochem. Photobiol.*, **B 1997**, 40, 3.

- [5] M. J. K. Selgrade, M. H. Repacholi, H. S. Koren, *Environ. Health Perspect.* **1997**, 105, 332.
- [6] R. Lucas, T. McMichael, W. Smith, B. Armstrong, *Solar ultraviolet radiation: Global burden of disease from solar ultraviolet radiation*, World Health Organization, Geneva, Switzerland **2006**.
- [7] D. H. Kim, N. S. Lu, R. Ma, Y. S. Kim, R. H. Kim, S. D. Wang, J. Wu, S. M. Won, H. Tao, A. Islam, K. J. Yu, T. I. Kim, R. Chowdhury, M. Ying, L. Z. Xu, M. Li, H. J. Chung, H. Keum, M. McCormick, P. Liu, Y. W. Zhang, F. G. Omenetto, Y. G. Huang, T. Coleman, J. A. Rogers, *Science* **2011**, 333, 838.
- [8] C. Dagdeviren, Y. Shi, P. Joe, R. Ghaffari, G. Balooch, K. Usgaonkar, O. Gur, P. L. Tran, J. R. Crosby, M. Meyer, Y. W. Su, R. C. Webb, A. S. Tedesco, M. J. Slepian, Y. G. Huang, J. A. Rogers, *Nat. Mater.* **2015**, 14, 728.
- [9] W. H. Yeo, Y. S. Kim, J. Lee, A. Ameen, L. K. Shi, M. Li, S. D. Wang, R. Ma, S. H. Jin, Z. Kang, Y. G. Huang, J. A. Rogers, *Adv. Mater.* **2013**, 25, 2773.
- [10] R. C. Webb, A. P. Bonifas, A. Behnaz, Y. H. Zhang, K. J. Yu, H. Y. Cheng, M. X. Shi, Z. G. Bian, Z. J. Liu, Y. S. Kim, W. H. Yeo, J. S. Park, J. Z. Song, Y. H. Li, Y. G. Huang, A. M. Gorbach, J. A. Rogers, *Nat. Mater.* **2013**, 12, 938.
- [11] M. Stoppa, A. Chiolerio, *Sensors* **2014**, 14, 11957.
- [12] G. Appelboom, E. Camacho, M. E. Abraham, S. S. Bruce, E.L.P. Dumont, B. E. Zacharia, R. D'Amico, J. Slomian, J. Y. Reginster, O. Bruyère, E. S. Connolly Jr., *Arch. Public Health* **2014**, 72, 28.
- [13] J. Kim, A. Banks, H. Y. Cheng, Z. Q. Xie, S. Xu, K. I. Jang, J. W. Lee, Z. J. Liu, P. Gutruf, X. Huang, P. H. Wei, F. Liu, K. Li, M. Dalal, R. Ghaffari, X. Feng, Y. G. Huang, S. Gupta, U. Paik, J. A. Rogers, *Small* **2015**, 11, 906.
- [14] J. Kim, A. Banks, Z. Q. Xie, S. Y. Heo, P. Gutruf, J. W. Lee, S. Xu, K. I. Jang, F. Liu, G. Brown, J. Choi, J. H. Kim, X. Feng, Y. G. Huang, U. Paik, J. A. Rogers, *Adv. Funct. Mater.* **2015**, 25, 4761.
- [15] P. Gutruf, E. Zeller, S. Walia, H. Nili, S. Sriram, M. Bhaskaran, *Small* **2015**, 11, 4532.
- [16] D. Kim, G. Shin, J. Yoon, D. Jang, S. J. Lee, G. Zi, J. S. Ha, *Nanotechnology* **2013**, 24, 31.
- [17] X. Sheng, C. Yu, V. Malyarchuk, Y. Lee, S. Kim, T. Kim, L. Shen, C. Horng, J. Lutz, N. C. Giebink, J. Park, J. A. Rogers, *Adv. Opt. Mater.* **2014**, 2, 314.
- [18] A. Chiolerio, I. Roppolo, V. Cauda, M. Crepaldi, S. Bocchini, K. Bejtka, A. Verna, C. F. Pirri, *Nano Res.* **2015**, 8, 1956.
- [19] H. Ito, *Adv. Polym. Sci.* **2005**, 172, 37.
- [20] R. Schwalm, *UV Coatings: Basics, Recent Developments and New Applications*, Elsevier, Amsterdam **2007**.
- [21] C. A. Poynton, *Digital Video and HD: Algorithms and Interfaces*, Morgan Kaufmann, Waltham, MA, USA **2012**.
- [22] L. Gao, Y. H. Zhang, V. Malyarchuk, L. Jia, K. I. Jang, R. C. Webb, H. R. Fu, Y. Shi, G. Y. Zhou, L. K. Shi, D. Shah, X. Huang, B. X. Xu, C. J. Yu, Y. G. Huang, J. A. Rogers, *Nat. Commun.* **2014**, 5, 4938.
- [23] I. Sage, *Liq. Cryst.* **2011**, 38, 1551.
- [24] D. Dolphin, Z. Muljani, J. Cheng, R. Meyer, *J. Chem. Phys.* **1973**, 58, 413.
- [25] SL13A (AMS AG) including temperature sensor, <http://ams.com/eng/Products/Wireless-Connectivity/Sensor-Tags-Interfaces/SL13A> (accessed: August 2013).
- [26] R. Xua, K.-I. Jang, Y. Ma, H.N. Jung, Y. Yang, M. Cho, Y. Zhang, Y. Huang, J. A. Rogers, *Extreme Mech. Lett.* **2015**, 1, 120.
- [27] K.-I. Jang, S. Y. Han, S. Xu, K. E. Mathewson, Y. Zhang, J.-W. Jeong, G.-T. Kim, R. C. Webb, J. W. Lee, T. J. Dawidczyk, R. H. Kim, Y. M. Song, W.-H. Yeo, S. Kim, H. Cheng, S. I. Rhee, J. Chung, B. Kim, H. U. Chung, D. Lee, Y. Yang, M. Cho, J. G. Gaspar, R. Carbonari, M. Fabiani, G. Gratton, Y. Huang, J. A. Rogers, *Nat. Commun.* **2014**, 5, 4779.